Delocalization and Stretch-Bend Mixing of the HOH Bend in Liquid Water

William B. Carpenter,[1] *Joseph A. Fournier,*[1] *Rajib Biswas,*[2] *Gregory A. Voth*[1] *and Andrei Tokmakoff*[1,a]

[1]*Department of Chemistry, James Franck Institute, and Institute for Biophysical Dynamics, The University of Chicago, Chicago, Illinois 60637, USA*

[2]*Solid State and Structural Chemistry Unit, Indian Institute of Science, Bangalore, India - 560012*

Abstract

Liquid water's rich sub-picosecond vibrational dynamics arise from the interplay of different high- and low-frequency modes evolving in a strong, yet fluctuating hydrogen bond network. Recent studies of the OH stretching excitations of H_2O indicate that they are delocalized over several molecules, raising questions about whether the bending vibrations are similarly delocalized. In this paper, we take advantage of an improved 50 fs time-resolution and broadband IR spectroscopy to interrogate the 2D IR line shape and spectral dynamics of the HOH bending vibration of liquid H_2O. Indications of strong bend-stretch coupling are observed in early-time 2D IR spectra through a broad excited state absorption which extends from 1500 cm^{-1} to beyond 1900 cm^{-1}, which corresponds to transitions from the bend to the bend overtone and OH stretching band between 3150 – 3550 cm^{-1}. Pump-probe measurements reveal a fast 180 fs vibrational relaxation time, which results in a hot-ground state spectrum that is the same as observed for water IR excitation at any other frequency. The fastest dynamical time scale is 80 fs for the polarization anisotropy decay, providing evidence for the delocalized or excitonic character of the bend. Normal mode analysis conducted on water clusters extracted from molecular dynamics simulations corroborate significant stretch-bend mixing and indicate delocalization of δ_{HOH} on 2-7 water molecules.

[a] Author to whom correspondence should be addressed. Electronic mail: tokmakoff@uchicago.edu. Telephone: (773) 834-7696

I. Introduction

Water is a remarkable liquid whose unusual properties arise from the complex behavior of its ordered yet fluctuating hydrogen bond (HB) network. The vibrational modes of water molecules in the liquid include high-frequency modes such as stretching and bending motions and lower-frequency intermolecular degrees of freedom such as librations, HB stretching and distortions of the HB network. Additionally, the HB interactions between molecules are strong enough that stretching and bending frequencies are heavily dependent on intermolecular configurations. Whereas water's intermolecular modes have long been described as highly collective,[1] high-frequency motions have traditionally been thought of as localized intramolecular vibrations. However, recent experiments[2–7] and theory[8–16] have demonstrated that short-pulse infrared excitation of OH stretching vibrations (ν_{OH}) in H_2O results in a vibrational exciton delocalized over multiple molecules. The strong intermolecular couplings between different ν_{OH} oscillators responsible for this delocalization also manifest themselves as rapid energy dissipation to low-frequency modes, orientational randomization, and decay of the frequency-frequency correlation function, all occurring on time scales faster than the structural relaxation of the liquid.

The bending vibration in water (δ_{HOH}) also has the potential to be delocalized as a result of intermolecular bend-bend interactions or coupling of the bend to the excitonic OH stretch. Recent simulations have examined the ultrafast vibrational dynamics[10,17–19] and delocalization of δ_{HOH}.[9,10,20] They modeled the rapid 200 fs vibrational relaxation of δ_{HOH}[21–24] and fast decay of the frequency-frequency correlation function (120 fs)[9] and concluded that δ_{HOH} is actually more delocalized than ν_{OH} in liquid H_2O.[20] While ν_{OH} is expected to delocalize over ~5 water molecules,[8,20] δ_{HOH} was predicted to delocalize over ~20 molecules, extending to the second solvation shell around a central water. Other computational studies also reproduced the fast vibrational relaxation processes and provided a detailed description of efficient and ultrafast transfer of bending energy in one molecule to librational motion of its solvation shell.[17–19] These

studies did not specifically account for intermolecular bend coupling needed to address delocalization.

Despite the wealth of experimental studies on ν_{OH} and recent theoretical predictions, experimental studies characterizing the ultrafast relaxation dynamics of δ_{HOH} in H_2O are sparse. Infrared pump-probe studies of the bend mode have observed the fast relaxation and strong coupling to ν_{OH},[21,25] and the 2D bend lineshape has been compared against the HOD bend in D_2O.[24] The OH stretch and HOH bend vibrations have been demonstrated to mix significantly due to the anharmonicity of their nuclear potentials.[2,3] Ultrafast nonlinear infrared (IR) spectroscopies have been instrumental in characterizing stretch-bend coupling, owing to the short time scales accessible in these experiments and the ability to detect these anharmonic interactions as cross peaks.[2,3,21,22,25,26] Delocalization of the bend vibration in H_2O remains to be experimentally addressed. A detailed 2D IR and polarization anisotropy study should be able to elucidate bending frequency correlations, the nature of the interaction with ν_{OH}, and the possible presence of delocalization.

In this paper, we take advantage of a 50 fs, 350 cm^{-1} bandwidth pump pulse and a broadband IR probe to accurately capture the fast dynamics of the bending vibration in liquid H_2O using two-dimensional infrared (2D IR) and polarization-dependent transient absorption (TA) spectroscopy. To highlight the strongly coupled environment of neat liquid H_2O, we contrast the bending modes of neat H_2O with the bending mode of H_2O monomers in acetonitrile. 2D IR and TA spectroscopy reveals an excited state absorption (ESA) of δ_{HOH} in neat H_2O that extends over the range of 1500-1900 cm^{-1}, which originates in the anharmonic nature of the coupled stretching and bending modes. We also observe an 80 fs anisotropy decay of δ_{HOH} in liquid H_2O, reminiscent of the anisotropy decay of the excitonic ν_{OH}. The fast decays and the strong mixing with the excitonic stretch suggest that the δ_{HOH} excitation is delocalized. DFT-based normal mode analysis of water clusters extracted from molecular dynamics simulations corroborate significant stretch-bend mixing and delocalization of δ_{HOH} on up to 7 water molecules.

II. Methods

A. Experimental Methods

2D IR spectroscopy was used to characterize the IR spectral dynamics and interactions of the water bending mode. The output of a Ti:Sapphire regenerative amplifier (Coherent, *Legend USX,*

800 nm, 5 mJ pulse energy, 1 kHz, 25 fs) is split into two paths with independent grating compressors. One path pumps a commercial two-stage optical parametric amplifier (Light Conversion, *TOPAS Prime*) to generate signal and idler pulses with wavelengths 1.4 μm and 1.8 μm, respectively. The collinear signal and idler pulses combine in a homebuilt difference frequency generation (DFG) setup in a 0.5 mm thick $AgGaS_2$ crystal cut at 42.7 degrees and tilted to phase match at 1685 cm^{-1} (5 μJ pulse energy, FWHM 350 cm^{-1}, 50 fs). The autocorrelation interferogram, extracted pulse time profile, and power spectrum are shown in Fig. S1 in the Supplementary Information. The interferometric autocorrelation was fit to the autocorrelation expression for a Gaussian pulse with linear chirp,[27] yielding center frequency of 1682 cm^{-1} and a pulse width of 51 fs. The second path pumps a homebuilt broadband IR source, which has been described in detail elsewhere.[28] Briefly, 500 μJ of the 800 nm pulses generated the second and third harmonics collinear with the 800 nm beam, which were focused into a gentle stream of nitrogen gas. The resulting plasma radiates broadband IR light centered at 2000 cm^{-1}, with bandwidth that allows us to probe from 1000 cm^{-1} to 4000 cm^{-1}, pulsewidth of 50 fs, and pulse energy of < 10 nJ.

The 6 μm pulses were aligned into a Mach-Zehnder interferometer equipped with two KBr beamsplitters and high-accuracy translation stages (Aerotech *ANT-25L)* to generate two pulse pairs. The pulses in each pulse pair are separated by an experimentally controlled time delay τ_1 with resolution of 0.3 fs, and the fixed arm is chopped at 500 Hz. One pulse pair passes through a tunable zero-order CdSe waveplate (*Alphalas)* and a ZnSe wire-grid polarizer (*Specac*) before focusing at the sample. The CdSe waveplate was chosen to minimize dispersion in the 6 μm region, since the zero-dispersion point is at 6 μm. The second pulse pair is sent to a single-pixel room temperature MCT detector which is used for collecting the interferogram of the pulses and for applying an automatic phase correction for the 2D IR spectra.[29]

The 2D IR spectra were collected in the pump-probe geometry,[30] with the 6 μm pulse pair serving as the pump, and the broadband IR source acting as the probe, with a controllable waiting time delay τ_2. The time delay is generated by another high-accuracy translation stage (Aerotech *ANT-25L*) in the broadband IR path. A gold parabolic mirror focuses the three pulses at the sample with spot size of 130 μm and generates a third-order nonlinear polarization in the sample, which radiates a signal field in the direction of the probe. After passing through an analyzing polarizer, the heterodyned signal is dispersed by a 50 groove/mm grating onto one stripe of a 2 × 64 pixel

MCT array detector (Infrared Systems). Half of the probe field is sent directly to the other stripe of the detector to serve as a reference pulse to correct for power fluctuations in the probe.

To collect the 2D IR signal at a single waiting time τ_2, the heterodyned signal was measured as a function of detection frequency (ω_3) as the pulse pair delay (τ_1) was stepped in 4 fs increments. For each point in τ_1 the signal was collected as a change in absorption of the probe beam as $\Delta A_i = -\log[(S_i/R_i)(R_{i+1}/S_{i+1})]$ where i is measured with the chopped arm open, $i+1$ is measured with the chopped arm closed, S_i is the signal from the sample, and R_i is the reference arm used to correct for fluctuations in probe intensity. For a fixed detection frequency ω_3, the resulting signal is an oscillating free induction decay (FID) with a constant offset from the pump-probe signal arising between the static arm and the broadband probe. The constant offset is subtracted and the FID is phased with the Mertz correction[31] determined from one output of the Mach-Zehnder interferometer. A Hann window is applied to the FID, and the data is zero padded before Fourier transformation along the τ_1 axis for each point in ω_3. This produces the excitation frequency axis, ω_1.

The 2D IR spectra were collected with magic angle (MA) polarization, and transient absorption (TA) spectra were collected with MA, ZZZZ (parallel), and ZZYY (perpendicular) polarization schemes. Polarizations were controlled by rotating the polarization of the pump-pulses with the CdSe waveplate, and keeping the polarization of the probe beam fixed. For the ZZZZ and ZZYY polarizations, we made sure to match the pump pulse power. For a given frequency in detection frequency ω_3, the anisotropy was calculated as $r(\tau_2) = (\Delta A_{ZZZZ} - \Delta A_{ZZYY}) / (\Delta A_{ZZZZ} + 2\Delta A_{ZZYY})$.

To minimize chirp and the nonresonant signal from the sample windows, we held samples of neat H_2O between two 200 μm thin CaF_2 windows (Crystran). We characterized the nonresonant response of the thin windows by taking TA spectra of D_2O sandwiched between the thin windows (~1 μm sample pathlength). Because the absorption of D_2O is minimal in the 6 μm region, the positive signal we observe at early waiting times corresponds to the signal from the windows. The data, presented in Fig. S2 in the Supplemental Information, demonstrate that chirp is insignificant in the desired frequency range. In order to assure that minimal nonresonant response contributed to our dataset, we only analyzed data taken after $\tau_2 = 100$ fs.[32]

The linear IR spectra were measured with an FTIR spectrometer equipped with an MCT detector (Bruker). For neat H_2O, 1 μL of sample was sandwiched between two 1 mm thick CaF_2 windows, such that the absorbance of ν_{OH} was approximately OD 1, corresponding to ~1 μm path

length. Neat H_2O samples were purified by reverse osmosis and ion exchange to 18 MΩ·cm resistivity (Millipore, *Milli-Q*). Dilute H_2O in acetonitrile (Acn) samples were prepared by diluting H_2O to 5% (by mole) in HPLC grade Acn (Sigma Aldrich), resulting in solutions of 1.6M H_2O. The dilute H_2O/Acn samples were placed between two 1 mm thick CaF_2 windows with a 50 μm Teflon spacer, such that the optical density of δ_{HOH} was ~0.4.

B. Simulation Details

To investigate the extent of delocalization of the water bending vibration, we performed a DFT-based normal mode analysis of water clusters drawn from molecular dynamics (MD) simulations. This builds on our recent study of the vibrational spectroscopy of water and aqueous protons, where the description of the computational details is provided.[33] Briefly, 500 clusters consisting of water molecules within 5Å of a central hydrogen (typically 18 molecules total) were drawn from a simulation of 256 SPC/Fw waters. Normal modes of the clusters determined from the Hessian of the potential energy were used to calculate a density of states and spectral density (IR transition dipole intensity weighted density of states) by averaging over all clusters. Adiabatic potential energy surfaces were calculated at the B3LYP 6-311++G(d,p) level and basis set using the Gaussian 09 package[34]. Normal modes of cluster vibrations were obtained from the eigenvectors e_i of the Hessian with frequency eigenvalues ω_i, and intensities of the normal modes were calculated as the square of the dipole moment (μ) derivative with respect to normal mode coordinate q_i,

$$I(\omega_i) = \left| \frac{d\mu}{dq_i} \right|^2 . \tag{1}$$

The normal mode analysis is shown as the spectral density, $\rho(\omega)$, averaged over the number of clusters, $N_{clusters}$,

$$\rho(\omega) = \frac{1}{N_{clusters}} \sum_{clusters} \sum_{\text{modes } i} I(\omega_i)\delta(\omega - \omega_i). \tag{2}$$

To analyze the delocalization of modes, the participation ratio PR_i of the i^{th} normal mode was calculated from the mode displacement vectors e_i as[35]

$$PR_i = \left[N \sum_{\alpha=1}^{3N} \left(e_i^{\alpha} \cdot e_i^{\alpha} \right)^2 \right]^{-1}, \tag{3}$$

where N is the total number of atoms in the cluster and α refers to the $3N$ Cartesian coordinates describing the atomic displacements for each normal mode. For reference, a local mode yields a $PR \approx N^{-1}$, whereas a fully delocalized mode will approach $PR=1$. As an alternative representation of delocalization, we also calculated the number of atoms, N_{atoms}, with $|e| \geq 0.1$ Å participating in each vibrational mode. To minimize the contribution of surface water molecules, we calculated the PR of only those normal modes which have non-zero contribution to the central water molecule for each water cluster. To analyze the vibrational character of each mode, we used HOH bond-angle changes of $\delta\theta_{HOH} > 1°$ and O-H bond length changes of $\delta r_{OH} > 0.01$ Å as cutoffs for determining whether a mode had bend character, stretch character, or both.

III. Results

A. Early-time 2D IR spectrum of H_2O

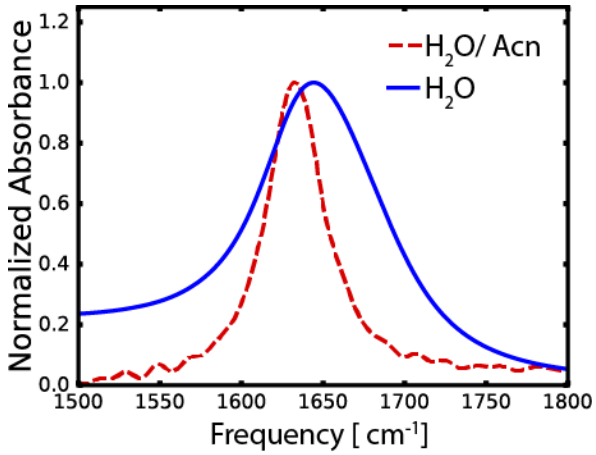

FIG. 1. The linear absorption spectrum of neat H_2O (solid blue), and 1.6M H_2O in Acn (dashed red). The H_2O/Acn spectrum is shown with Acn solvent subtracted.

To highlight the effect of the HB network on the HOH bending vibration, we first contrast the FTIR spectrum of neat H_2O with the 2D IR spectrum of 1.6M H_2O in acetonitrile (Fig. 1). At this concentration in Acn, water is solvated primarily in the monomer form which forms relatively weak HBs to the CN moieties of the solvent.[36,37] In the FTIR spectrum, the frequency of the bend resonance red-shifts and narrows in linewidth (ω_{HOH} = 1630 cm^{-1}, 40 cm^{-1} FWHM) compared to the neat liquid (ω_{HOH} = 1650 cm^{-1}, 85 cm^{-1} FWHM).[37,38] Previous simulations of the bend in neat H_2O have demonstrated that the bend exhibits non-Gaussian frequency fluctuations, and the lineshape broadens due to intermolecular coupling.[39]

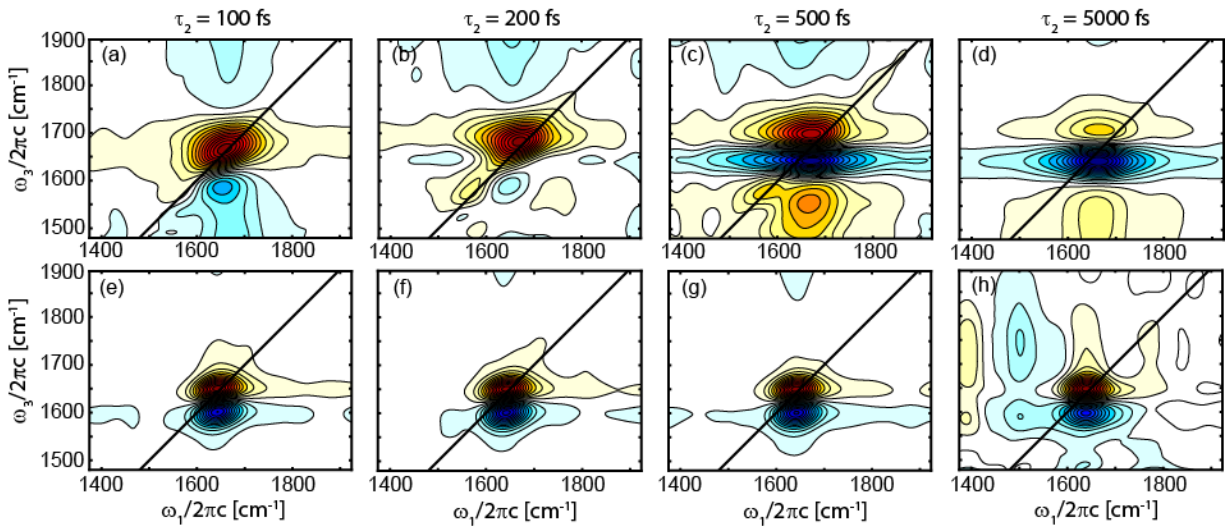

FIG. 2. The 2D IR waiting time series of δ_{HOH} for (a) – (d) neat H_2O and (e) – (h) water monomers in acetonitrile. The bend feature at τ_2 = 100 fs in neat H_2O displays a broad ESA that flanks the GSB. Each spectrum has been individually normalized to the feature with the maximum absolute amplitude. The low signal to noise ratio in panel (h) is due to decreased amplitude from population relaxation. H_2O/Acn spectra are shown without Acn subtraction.

The 2D IR spectrum of H_2O at early waiting time (τ_2 = 100 fs) is presented in Fig. 2a. The 2D IR spectra of δ_{HOH} in 1.6M H_2O/Acn display a doublet typical of a weakly anharmonic mode, with a positive ground state bleach (GSB) of the 0→1 transition at 1630 cm^{-1} on the diagonal, and a negative 1→2 excited state absorption (ESA) anharmonically red shifted to ω_3 = 1600 cm^{-1}. The peaks are roughly equal in intensity and linewidth and show no diagonal elongation, implying homogeneous broadening. The characteristics of these peaks exemplify what one would expect for a weakly anharmonic bend vibration,[40] with weak interactions between the H_2O monomer and the Acn solvent.

By contrast, the associative nature of neat water's HB network results in a dramatic change in the 2D IR spectrum of the HOH bend in neat H_2O (Fig. 2a). As expected for a stronger HB interaction, the GSB of δ_{HOH} at 1650 cm^{-1} is blue shifted compared to δ_{HOH} of the H_2O monomer in Acn. Although its linewidth is 100 cm^{-1}, the bleach spreads from ω_1 <1500 cm^{-1} to >1800 cm^{-1}. The ESA presents as a negative feature red shifted with respect to the GSB, peaked at ω_3 = 1590 cm^{-1}, consistent with a 55 cm^{-1} anharmonicity reported previously.[41] The ESA exhibits a long tail to the red in ω_3,[42] which is absent in the spectrum of monomeric H_2O. We also observe an additional ESA that arises from excitation of δ_{HOH} which is blue shifted in ω_3 from the GSB and spans ω_3 = 1750 – 1900 cm^{-1}. The 2D IR spectrum at higher detection frequencies reveals that

the ESA continues up to ω_3 = 2800 cm^{-1}, beyond the bend-libration combination band around 2100 cm^{-1} (Fig. S3 in the SI). It is likely that the two ESAs we observe arise from one extremely broad induced absorption whose intensity interferes with the GSB. As a result, it is difficult to say whether the diagonal broadening of the GSB line shape reflects inhomogeneous broadening. As one feature, the ESA stretching from ω_3 = 1500-1900 cm^{-1} would correspond to excitation from the δ_{HOH} singly excited state at ω = 1650 cm^{-1} to excited states spanning the stretch and bend overtone region: 3150-3550 cm^{-1}. Our data on the GSB are similar to previously reported 2D IR spectra of δ_{HOH}.[24] However, the broader frequency pulses used in this dataset enable us to characterize the breadth of the bleach in ω_1 and the length of the ESA in ω_3.

We also observe a diagonal bleach at 1570 cm^{-1}, most clearly visible at τ_2 = 500 fs but also present at τ_2 = 100 fs and 200 fs. Although a narrow resonance is not clearly present in the linear absorption spectrum, the feature could be a weak resonance such as a hot band hidden within the broad background on the low frequency wing of the δ_{HOH} absorption.[43–45] Since it aligns in ω_3 with the bend ESA, one might expect this signal to arise from a fifth order nonlinear process that drives the system higher up the vibrational ladder.[46,47] If so, its amplitude is expected to grow quadratically with pump intensity. Given the weak signal and limited range of available pump energy at the sample, we were unable to conclusively determine if the intensity dependence of the feature is nonlinear.

B. Waiting time dependence of 2D IR spectra of H_2O

We next focus on the waiting time series of the bending features of neat and monomeric H_2O in Fig. 2. In 1.6M H_2O/Acn, the GSB and ESA slowly decay to zero amplitude with the same rate and with negligible change in line shape, typical for traditional vibrational relaxation of a homogeneous lineshape. For neat H_2O, however, the intensity and lineshape rapidly evolve throughout the spectrum, which we quantify by tracking integrated intensities for several features in Fig. 3. The GSB decays as an exponential with a 180 fs time scale, which is within the literature range of 170 – 260 fs.[21,22,24] For the induced absorption features, the lower-frequency portion (ESA_2) decays in 150 fs, while the blue-shifted component (ESA_1) decays in 110 fs. This is consistent with the notion that these features are of similar origin, both tracking efficient dissipation into lower-frequency modes.

In addition to fast relaxation processes, all integration windows are influenced to varying extents by a common 840 fs exponential rise, due to a signal that rises to a constant plateau after ~3 ps. This signal represents the change in absorption of δ_{HOH} after the energy from the pump pulse dissipates into low-frequency modes and is referred to as the "hot ground state" (HGS).[22,32,48–50] The long-time spectral shape which results from the growth of the HGS signal is invariant in ω_1, which demonstrates that the energy dissipation has randomized the initial excitation. As such, each intensity decay was fit with a common second exponential with an 840 fs time scale, determined by the frequency window bounded in purple in Fig. 3, and is comparable to other measurements.[2,3,21,26,42,49] This window shows minimal amplitude from the δ_{HOH} GSB but substantial response from the HGS. While the decays of the GSB and ESA portions were normalized to the initial value in Fig. 3,the HGS is displayed as a rise to large positive signal (ω_3 = 1650 cm^{-1} in Fig. 2d) to highlight the rising nature of the HGS. Because the HGS signal varies in intensity across different integration regions, the amplitude of the HGS component varies in each biexponential decay. This is evident in the traces of ESA_1 and ESA_2, where the relative HGS amplitudes are 36% and 16% respectively, giving the misleading appearance of a slower decay of ESA_1. Regardless, the fast decay time scales of the two ESA regions are distinct within error.

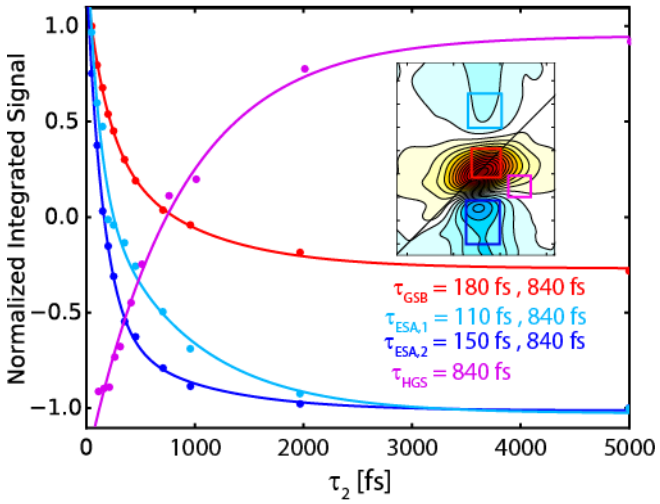

FIG. 3. Time dependence of integrated intensity of the main features in the 2D IR spectrum of neat H_2O. Inset: 2D IR spectrum of H_2O with colored squares indicating integration intervals for the respective colored lines. The features were integrated with the following (ω_1,ω_3) spectral ranges: GSB = (1640-1710 cm^{-1}, 1650-1710 cm^{-1}), ESA_1 = (1620-1700 cm^{-1}, 1750-1825 cm^{-1}) ESA_2 = (1620-1700 cm^{-1}, 1500-1590 cm^{-1}), and HGS = (1750-1800 cm^{-1}, 1600-1650 cm^{-1}).

C. Transient absorption spectra and pump-probe anisotropy decay of δ_{HOH}

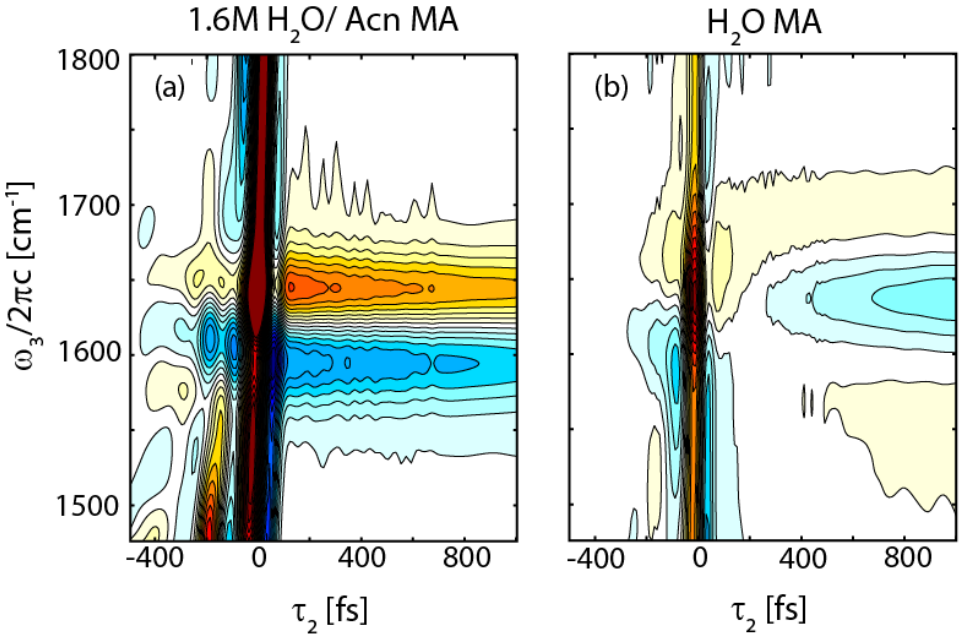

FIG. 4. Transient absorption spectra of δ_{HOH} in (a) 1.6M H_2O/ Acn and (b) neat H_2O in the magic angle polarization scheme. Orange features correspond to negative absorption, and blue features correspond to positive absorption. At $\tau_2 = 0$ in both spectra, there is a stripe of bleach along all ω_3, which corresponds to nonresonant response from the CaF_2 windows.

In Fig. 4a and 4b, we present the magic angle TA spectra for H_2O in Acn and in neat H_2O, respectively. In 1.6M H_2O/Acn, the GSB (ω_3=1640 cm^{-1}) and ESA (ω_3=1590 cm^{-1}) decay exponentially with the same 2.4 ps time scale (Fig. 5). In neat H_2O, the early-time features such as the GSB centered at ω_3 = 1650 cm^{-1} and ESA stretching from ω_3 = 1500 – 1850 cm^{-1} decay rapidly in 170 fs and 140 fs, respectively, followed by an 840 fs rise of the HGS signal. To effectively contrast the fast decays in neat H_2O with the slower relaxation of monomers in Acn, we plot the TA decays in Fig. 5. Traces have been normalized to the initial time point $S(0)$ after subtracting the frequency-dependent value of the HGS spectrum at long times, $S(\infty,\omega_3)$:

$$\Delta S(\tau_2,\omega_3) = \frac{S(\tau_2,\omega_3) - S(\infty,\omega_3)}{S(0,\omega_3) - S(\infty,\omega_3)}. \quad (4)$$

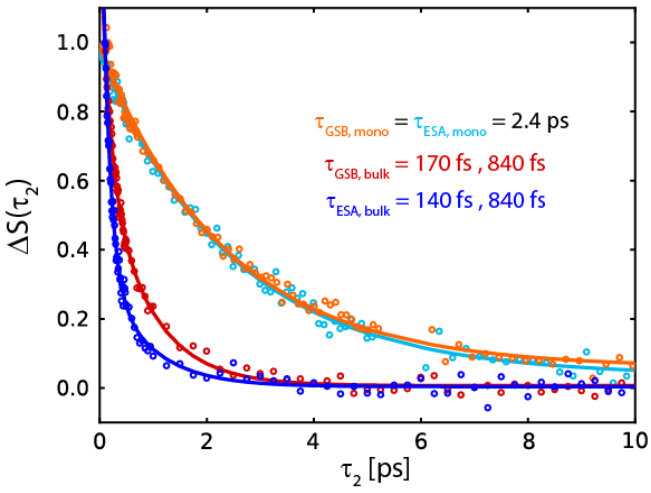

FIG. 5. Time dependence of integrated intensity of the main features in the TA spectra of neat H_2O and H_2O monomers in acetonitrile. The features were integrated with the following ω_3 spectral ranges: GSB, bulk = 1650-1710 cm^{-1}; ESA, bulk = 1500-1590 cm^{-1}; GSB, mono = 1620-1670 cm^{-1}; ESA, mono = 1590-1610 cm^{-1}.

At τ_2 = 5 ps, the TA spectrum closely resembles a temperature difference FTIR spectrum of H_2O (Fig. S4 in the SI), similar to observations of the HGS spectrum when other water resonances are excited and allowed to relax.[2,3,22,25] Both the temperature difference spectrum and the HGS spectrum result from an overall weakening of the HB network. There is a weak bleach feature centered at ω_3 = 1550 cm^{-1}, an induced absorption centered at ω_3 = 1620 cm^{-1}, with a weak bleach centered at ω_3 = 1690 cm^{-1}. This bleach/induced absorption/bleach pattern is consistent with the red-shifting and narrowing of δ_{HOH}. For the bending mode, then, this implies that weakening the HBs results in a slightly more homogeneous environment. The HGS spectrum and the temperature difference spectrum vary slightly on the low frequency side, which suggests subtle differences between thermal heating of the sample and sub-ps energy dissipation into low-frequency modes.

Pump-probe anisotropy decays were calculated from parallel and perpendicular polarization TA experiments after correcting for the growth of the HGS.[49,51,52] Since the HGS spectrum grows in uniformly for all ω_3, we generated a surface describing the HGS growth by scaling the long-time pump-probe trace with an exponential rise:

$$S_{HGS}(\tau_2, \omega_3) = [1 - \exp(-\tau_2 / \tau_{HGS})]S(\infty, \omega_3), \quad (5)$$

where τ_{HGS} = 840 fs. The difference of S_{HGS} from the neat H_2O TA surface (Fig. S4 in the SI) corrects for the isotropic HGS signal and removes a zero-crossing in the denominator of the anisotropy expression.

The resulting ZZZZ and ZZYY TA traces from ω_3 = 1645-1655 cm^{-1} (Fig. 6a) yield the pump-probe anisotropy in Fig. 6b. The anisotropy decay was fit to an exponential with a floating offset to qualitatively capture the decay dynamics, even though the data demonstrate that the anisotropy is not the best described with a single exponential. Regardless, the anisotropy decays rapidly and monotonically with a e^{-1} time scale of 80 fs. As a way to obtain a mean relaxation time, the first moment of the relaxation curve was calculated to be 120 fs, which is similarly rapid. This fast decay is similar in time scale to the anisotropy decay of the OH stretching vibration in H_2O.[3] Additionally, a shoulder and a beat arise at τ_2 = 65 fs in the ZZZZ and ZZYY traces, respectively, which corresponds roughly to a librational period. These features are not retained in the anisotropy, nor are they present in the magic angle decay, which only reports on population relaxation dynamics. To contrast, we also present the pump-probe anisotropy decay of δ_{HOH} in 1.6M H_2O/Acn, which decays on 240 fs and 2.2 ps time scales (Fig. 6d). The long time scale roughly agrees with the reorientation of neat Acn,[53] and the fast time scale agrees with the fast anisotropy decay component seen for the OH stretches in the H_2O monomer, previously attributed to intramolecular energy transfer.[37] The 2.2 ps time scale has also been observed in the anisotropy decay of the OH stretches of the H_2O monomer and has been attributed to the reorientation of H_2O in Acn.[37]

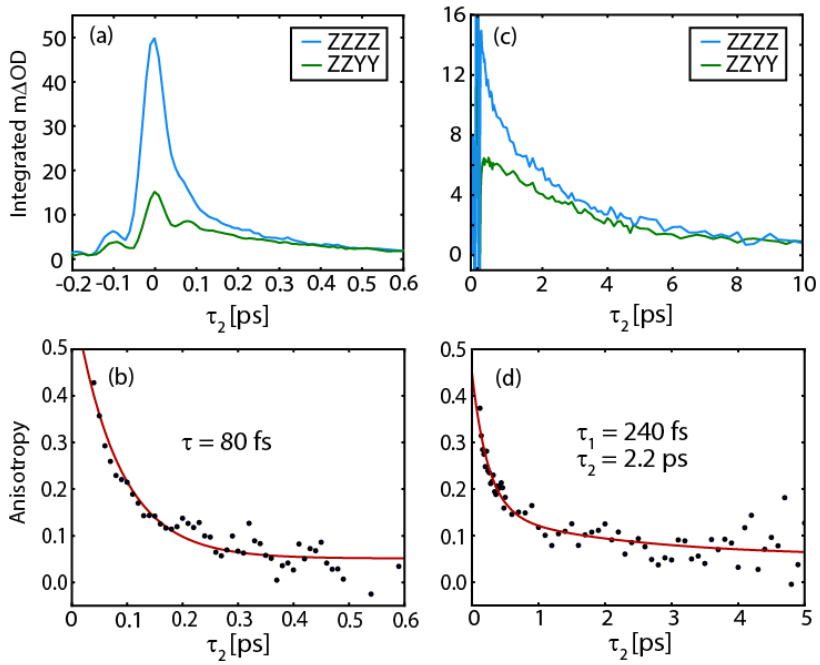

FIG. 6. (a) TA traces for δ_{HOH} in ZZZZ polarization scheme (solid blue) and ZZYY scheme (dashed green) over the range ω_3 = 1645 cm^{-1} – 1655 cm^{-1}. (b) Pump-probe anisotropy decay of δ_{HOH}. (c) ZZZZ and ZZYY traces of δ_{HOH} for monomers in Acn. (d) Pump-probe anisotropy decay of δ_{HOH} for monomers in Acn.

IV. Discussion

A. The 2D IR Spectrum of δ_{HOH}

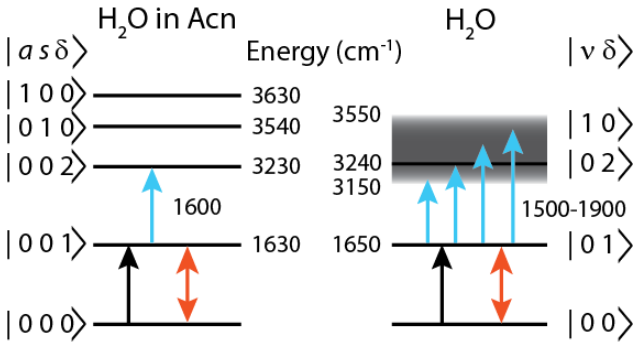

FIG. 7. Energy level diagram for transitions observed in the 2D IR spectra. (Left) Energies of the asymmetric (*a*) and symmetric stretch (*s*) and bend (δ) vibrations of H_2O monomers in Acn. (Right) Bend (δ) and stretch (ν) exciton states in neat H_2O. Black arrows correspond to pump excitation of δ_{HOH}. Probing step is illustrated as double-headed orange arrows for the GSB, and blue arrows for the ESA. In H_2O monomers, we do not observe an ESA to stretches, but in neat H_2O ESA to the extremely broad ν_{OH} is indeed observed.

The 2D IR spectroscopy of the bending vibration of liquid H_2O is dramatically different from that of H_2O monomers in acetonitrile. The 2D lineshape of the GSB in neat H_2O broadens substantially along and against the diagonal, indicating both faster dephasing and a larger distribution of local HB environments. While the GSB and the ESA of the monomer bend are the same width, the ESA of the bend in neat H_2O is extensively broadened in ω_3. Previously, we also observed extreme broadening of the absorption induced by exciting the OH stretching vibration of H_2O, with an ESA that spread from a peak near 3000 cm^{-1} to <1500 cm^{-1}.[2,3] For the case of ν_{OH}, the ESA reflected the large vibrational anharmonicity originating in the HB network in addition to stretch-bend coupling via Fermi resonance, which resulted in transitions from a stretch exciton band to doubly excited states with stretch and bend character.

The interpretation of the broad ESA for the H_2O bend observed here has origins in the same anharmonic interactions, but manifests itself somewhat differently in the 2D spectrum. The greatest ESA intensity is located at ω_3 = 1590 cm^{-1}, which indicates that the most facile transition is directly to the bend overtone. However, this is a small part of an induced absorption that spreads from <1500 cm^{-1} to >1900 cm^{-1}. After accounting for the ω_1 = 1650 cm^{-1} excitation frequency, the blue-shifted ESA extending from ω_3 = 1750-1900 cm^{-1} corresponds to a band of vibrational states with energy 3400-3550 cm^{-1}, the frequency of the ν_{OH} fundamental band in the linear IR spectrum. The ESA to the bend overtone (~3240 cm^{-1}) is also merged with the stretching band in the linear IR spectrum, as a result of the ~2:1 Fermi resonance between stretch and bend frequencies.[54,55] Therefore, it is reasonable to consider that the two ESAs that we observe are actually two regions of one broader ESA, with a breadth that reflects the stretching band of the linear IR spectrum, as shown in Fig. 7.

While the bend-to-stretch ESA is initially surprising, it is not completely unexpected in hindsight and is even observable in previous experiments and simulations. The feature is not expected for weakly anharmonic modes since transitions from one quantum of one normal mode to one quantum of another normal mode is forbidden in the harmonic limit, but the strong anharmonicity imbued upon the modes from the HB network relaxes this selection rule. Upon closer inspection of previous reports of δ_{HOH}, the extended ESA is visible in vibrational pump-probe spectra of δ_{HOH}[22] and non-equilibrium molecular dynamics simulations of the 2D IR spectrum of δ_{HOH} using the flexible and polarizable TTM3-F potential.[10]

Given the unusual nature of the initial excitation, the relaxation of the bend is not readily described by simple relaxation pathways. For H_2O monomers in acetonitrile, both the GSB and ESA of δ_{HOH} relax in 2.4 ps, which is typical for simple dissipation of a weakly anharmonic mode. Similar behavior with longer lifetimes is observed for H_2O monomers in chloroform,[56] which indicate the important role that intermolecular interactions play in mediating vibrational relaxation.[57] By contrast, in neat H_2O the GSB of the bend decays in 180 fs, and the ESA decays slightly faster. The influence of the water HB network are also apparent when considering the δ_{HOH} relaxation time of ~400 fs for the δ_{HOH} vibration of quasi-monomeric H_2O in a 6M solution of H_2O in D_2O.[41] Non-equilibrium simulations of bend vibrational relaxation in H_2O attribute the fast relaxation to dissipation into high frequency librations primarily of the first solvation shell.[17,18] When the solvent is treated fully flexibly, this fast relaxation also includes transfer of bend excitation to δ_{HOH} modes on neighboring molecules, which is comparable to the rate of stretch-to-bend relaxation.[10] The mixing of the stretch and bend vibrations is clearly seen in the stretch-bend crosspeak of H_2O.[2,3] We also note the signature of more complex mixing of bend, stretching, and libration vibrations apparent from the uphill 2D cross-peak in which H_2O excitation between 1300-1500 cm^{-1} leads to immediate (τ_2 = 100 fs) crosspeaks to the stretch and bend overtone region at 3000-3700 cm^{-1}.[58] The combination of the experimental observables and relaxation simulations indicates that all inter- and intramolecular degrees of freedom in H_2O are intertwined, resulting in the observation of similarly fast relaxation processes regardless of excitation or detection frequency.

B. The Excitonic Nature of δ_{HOH}

Strong intermolecular couplings mean that excitation of the water bending transition with a short, broad bandwidth pump pulse enables coherent excitation of multiple interacting water molecules. In the neat liquid, all bend transitions are resonant, and thus, the bend excitation consists of a superposition of oscillations whose dipoles have a component along the polarization of the pump's electric field. The rapid δ_{HOH} anisotropy decay demonstrates that this coherence quickly randomizes its orientation, much faster than both the 180 fs lifetime and the 1.5 ps time scale of molecular rotation. By contrast, experiments on the H_2O monomer in Acn result in a local mode excitation that reorients in 2.2 ps as a result of diffusive molecular rotation. This anisotropy also includes an additional faster component arising from excitation reorientation due to

intramolecular mixing of the bend, symmetric stretch, and antisymmetric stretch, in close agreement with the OH stretch anisotropy decay for H_2O in Acn previously measured.[37] In the case of neat H_2O, the extremely rapid anisotropy decay has been observed several times with the OH stretch, and attributed to intermolecular interactions that scramble the direction of the initial excitation, either as a result of excitation hopping between molecules or excitonic interactions.[2–4,6,11,12,59,60] Given that the anisotropy of the bend occurs on a on the time scale of librations (the fastest intermolecular motions of the liquid),[61] and that the bend is strongly coupled with the other vibrations, our results point toward a collective excitonic excitation which evolves with liquid dynamics. Similar arguments have been used to explain the ultrafast anisotropy relaxation of the excitonic ν_{OH} as well.[2,3,12]

Because the bend couples strongly with the excitonic stretch, it may not be entirely surprising that the bend behaves excitonically as well. In both of these modes, the HB network is the common infrastructure that couples adjacent oscillators. Similarly, librational motion is the common mechanism that induces rapid randomization of the transition dipole, even without reorientation of individual molecules. This leads to the question of how delocalized the bend might be. Previous simulations suggest that δ_{HOH} delocalizes over more molecules than ν_{OH}.[20] Assuming that water vibrations lie in an intermediate coupling regime in which the strength of intermolecular interactions are of the same scale as the energetic disorder, we might expect that the vibrational delocalization scales with the distribution of vibrational frequencies. This was demonstrated in the 2D depolarization surface of ν_{OH}, which displayed a lower depolarization ratio for strongly hydrogen-bonded stretches, versus higher delocalization for stretches of intermediate frequency.[3] In comparison to the bend, the OH stretching frequency is particularly sensitive to the HB environment. Thus, for bends, it is possible that a narrower frequency distribution results in higher delocalization.

Compared to the bend of the H_2O monomer, however, the linear IR feature for δ_{HOH} in liquid water is broadened due to hydrogen bonding frequency shifts *and* intermolecular coupling. In a previous mixed quantum/classical analysis of the HOH bend, intermolecular couplings were necessary to accurately calculate the FTIR spectrum of δ_{HOH} in neat H_2O.[39] Setting the intermolecular coupling to zero also accurately reproduced the spectrum of the HOH bend for dilute H_2O in D_2O. While this analysis did not quantify the extent of delocalization of δ_{HOH}, it

nonetheless demonstrated that bending motions on nearby molecules resonantly couple with each other, resulting in a dramatic change in the lineshape of the bend.

C. Simulation of the Mode-Mixing and Delocalization of δ_{HOH}

To further investigate the extent of delocalization of the water bending vibration, we performed a DFT-based normal mode analysis of water clusters drawn from molecular dynamics (MD) simulations. The results of these calculations are presented in Fig. 8. The spectral density (Fig. 8a) shows three main peaks centered at 1000 cm^{-1}, 1730 cm^{-1}, and 2900 cm^{-1}, which are assigned as librations, δ_{HOH}, and ν_{OH} resonances. These peaks differ from experimental frequencies primarily as a result of DFT overestimating HB strength.[62] The bending modes primarily have pure bend or mixed stretch-bend character, as expected. On the other hand, stretching modes are primarily pure stretch character; however, modes with bending and mixed stretch-bend character appear on the low frequency side of the band, where the overtone of δ_{HOH} is expected. Furthermore, the librational band clearly has stretch and bend character associated with it, emphasizing the highly coupled nature of these vibrations.

The participation ratio (*PR)* is characterized as a function of vibrational frequency in Fig. 8b. The mean *PR* reaches a maximum at the center of each vibrational band and decreases with increasing mode frequency when comparing the stretch, bend, librational, and intermolecular (<500 cm^{-1}) peaks. The variance in the *PR* is large and also reaches a maximum coincident with the peaks in the spectral density. As a complement, the delocalization in terms of N_{atoms} participating in the normal mode is presented in Fig. 8c, which shows the same trends as the *PR*.

Focusing on the bending vibration (insets of Fig. 8c), these calculations reinforce that δ_{HOH} is delocalized over multiple water molecules. They indicate that the center of the band (1730 cm^{-1}) is more delocalized than the wings (1620 cm^{-1} and 1800 cm^{-1}), with a PR corresponding to 6-21 atoms. This value is about half the value predicted from a previous normal mode analysis of δ_{HOH},[20] but roughly corresponds to delocalization over a central molecule and its first solvation shell, consistent with *ab initio* MD simulations of spatially-resolved IR spectra of H_2O.[63] We also observe that δ_{HOH} is more delocalized than ν_{OH}, which involves on average ~6 atoms, a value that is low compared to literature.[8] Frozen cluster normal mode analysis will tend to underestimate the degree of delocalization due to a large fraction of molecules residing at the cluster surface. Taken

together, however, these calculations, theoretical studies, and our experimental findings indicate that that the H_2O bending vibration delocalizes over multiple molecules.

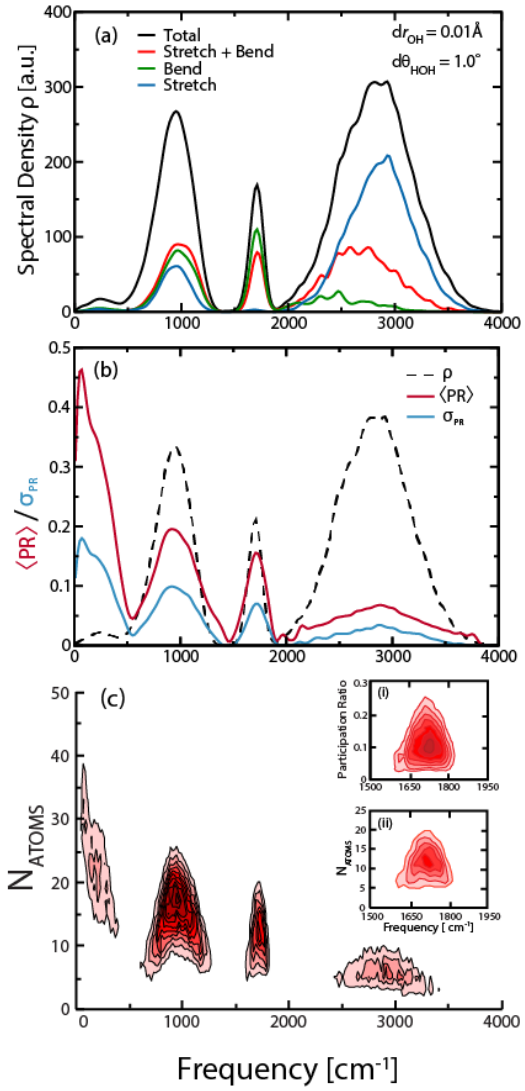

FIG. 8. (a) Spectral density for 5Å-cutoff water clusters, decomposed by stretch/bend character. The total spectral density is shown in black, stretch-only modes (δr_{OH} > 0.01 Å and $\delta\theta_{HOH}$ < 1°) are shown in blue, bend-only modes (δr_{OH} < 0.01 Å and $\delta\theta_{HOH}$ > 1°) are shown in green, and stretch-bend mixed modes (δr_{OH} > 0.01 Å and $\delta\theta_{HOH}$ > 1°) are shown in red. δ_{HOH} shows significant mixing of stretch and bend character, but very little pure stretch character. (b) Mean ⟨PR⟩ and standard deviation $\sigma_{PR} = [\langle PR^2\rangle - \langle PR\rangle^2]^{1/2}$ of the participation ratio as a function of vibrational frequency. (c) Number of atoms participating in the normal modes of H_2O. Inset i: The participation ratio of the δ_{HOH} normal mode, which is highest in the center of the band and lowest on the wings. Inset ii: Number of atoms participating in the δ_{HOH} normal mode, which follows the same trend as the participation ratio.

D. The Hot Ground State

The delocalization of δ_{HOH} goes hand-in-hand with the fast vibrational relaxation observed. After preparing the initial delocalized bend excitation, small amplitude changes of the extended hydrogen bond network allow the excitation to migrate and localize among bending motions of nearby molecules. Simultaneously, there is a likelihood on any given molecule that the energy can relax to librational motions, which further contributes to ultrafast energy dissipation. Because the excitation is delocalized over multiple molecules, relaxation involves many parallel channels that are together far more efficient than relaxation from a localized mode. The net result is that energy is dissipated into low frequency modes such as librations, hydrogen-bond stretches and distortions of the HB network, which is spectroscopically observed as the growth of the HGS.

The appearance of the HGS signal mimics a temperature difference spectrum since both spectra reflect overall HB weakening. When temperature is increased, HBs weaken on average due to the increase in randomized thermal motions, and the change in HB environment manifests as spectral shifts and changes in intensity. Remarkably, the HGS signal rises on an ultrafast, 840 fs time scale in liquid H_2O (Fig. 3), which suggests that the signal we observe is not a new equilibrium characterized by a Boltzmann distribution at an elevated temperature. Rather, the system is still in a highly nonequilibrium state characterized by a net excess of kinetic energy in the low-frequency intermolecular vibrations,[10,64,65] and the 2D IR measurement is sensitive to this weakened HB network.[3]

The time scale of HGS growth in H_2O has been measured to be ~800 fs, regardless of the measurement method or the initial mode excited.[3,21,23,24,42,49,66] This observation is inconsistent with a purely cascading relaxation mechanism between weakly coupled stretch and bend modes, which would predict a HGS growth time scale that is longer for stretch excitation than bend excitation. The 800 fs time scale lies between the vibrational lifetime (~200 fs) in neat liquid water and collective molecular rotation (1.5 ps),[49] and has been modeled with frequency resolved transient kinetic energy analysis.[64,67] In that framework, librational excitations relaxed to low frequency intermolecular motions, such as the stretching and distortion of hydrogen bonds and collective reorganization of the HB network, predicted to occur in 790 fs. In our interpretation stretch, bend, and librations are intimately coupled, and that any IR vibrational excitation seamlessly drives intermolecular motions of the HB network.

V. Summary and Conclusions

We have used ultrafast 2D IR and pump-probe spectroscopy to explore the ultrafast dynamics of the bending vibration in liquid H_2O. Anharmonic interactions result in strong mixing of bend and stretch, as demonstrated by the ESA transition between these bands. The 80 fs pump-probe anisotropy decay is extremely rapid compared to the 180 fs bend lifetime and the 1.5 ps hydrogen bond reorganization time. The HB network induces anharmonic coupling between adjacent molecules with sufficient strength such that the initial excitation is delocalized over multiple molecules, and the orientation of the bend dipole is quickly scrambled by librational oscillation. Cascading relaxation from highest frequency to lowest frequency modes does not capture the full extent of the dynamics observed in H_2O. Strong couplings also allow bend excitation to drive stretching motions (up-pumping), in addition to efficient downhill relaxation from the bend to low-frequency modes.

Many questions remain regarding the delocalized nature of high frequency vibrations in water, which leaves challenges for experiment and theory. What experimental tests can be used to quantify the extent of delocalization of high frequency vibrational excitations and follow these in a time-resolved manner? Existing experiments provide evidence for vibrational excitons, but are difficult to translate into a microscopic picture. Theoretical studies are needed to provide a molecular picture of the exciton dynamics, including the initially prepared state, spatial transport, localization, and dissipation. Previous non-equilibrium simulations of δ_{HOH} dissipation have excited only one water molecule; however, bend excitation by an infrared electromagnetic field should take delocalization into account,[5] perhaps using non-equilibrium simulations with an explicit pulsed external field.[68–70] Addressing delocalization effects may also help resolve differences in conclusions regarding how the excited bend energy is partitioned to other modes.[10,19,71] Additional relaxation channels are present and should also be considered, such as Fermi resonances (both intra- and intermolecular) and nonadiabatic dynamics involving vibrational conical intersections.[72] We hope that the present experiments will work spur interest in modeling these topics. Unravelling these dynamics could potentially lead to a rich description of a class of vibrational dynamics of a very different nature than most solution phase problems.

Supplementary Material

See supplementary material for pump pulse temporal and spectral characterization, characterization of window nonresonant response, the τ_2 = 100 fs neat H_2O 2D IR surface over the detection frequencies ω_3 = 1200-2800 cm^{-1}, and polarization dependent TA surfaces.

Acknowledgements

This work was funded by the Office of Basic Energy Sciences, U.S. Department of Energy (DE-FOA-0000995). J.A.F. thanks the Arnold O. Beckman Foundation for support through a postdoctoral fellowship.

References

[1] M. Cho, G.R. Fleming, S. Saito, I. Ohmine, and R.M. Stratt, J. Chem. Phys. **100**, 6672 (1994).
[2] K. Ramasesha, L. De Marco, A. Mandal, and A. Tokmakoff, Nat. Chem. **5**, 935 (2013).
[3] L. De Marco, J.A. Fournier, M. Thämer, W. Carpenter, and A. Tokmakoff, J. Chem. Phys. **145**, 94501 (2016).
[4] A. Paarmann, T. Hayashi, S. Mukamel, and R.J.D. Miller, J. Chem. Phys. **130**, 204110 (2009).
[5] Y. Nagata, S. Yoshimune, C.-S. Hsieh, J. Hunger, and M. Bonn, Phys. Rev. X **5**, 21002 (2015).
[6] D. Kraemer, M.L. Cowan, A. Paarmann, N. Huse, E.T.J. Nibbering, T. Elsaesser, and R.J.D. Miller, Proc. Natl. Acad. Sci. U.S.A. **105**, 437 (2008).
[7] S.T. van der Post, C.-S. Hsieh, M. Okuno, Y. Nagata, H.J. Bakker, M. Bonn, and J. Hunger, Nat. Commun. **6**, 8384 (2015).
[8] B.M. Auer and J.L. Skinner, J. Chem. Phys. **128**, 224511 (2008).
[9] S. Imoto, S.S. Xantheas, and S. Saito, J. Chem. Phys. **139**, 44503 (2013).
[10] S. Imoto, S.S. Xantheas, and S. Saito, J. Phys. Chem. B **119**, 11068 (2015).
[11] H. Torii, Chem. Phys. Lett. **323**, 382 (2000).
[12] T. l. C. Jansen, B.M. Auer, M. Yang, and J.L. Skinner, J. Chem. Phys. **132**, 224503 (2010).
[13] J.H. Choi and M. Cho, J. Chem. Phys. **138**, (2013).
[14] V. Buch, T. Tarbuck, G.L. Richmond, H. Groenzin, I. Li, and M.J. Shultz, J. Chem. Phys. **127**, 204710 (2007).
[15] C. Falvo, B. Palmieri, and S. Mukamel, J. Chem. Phys. **130**, 184501 (2009).
[16] L. Shi, J.L. Skinner, and T. la C. Jansen, Phys. Chem. Chem. Phys. **18**, 3772 (2016).
[17] R. Rey, F. Ingrosso, T. Elsaesser, and J.T. Hynes, J. Phys. Chem. A **113**, 8949 (2009).
[18] F. Ingrosso, R. Rey, T. Elsaesser, and J.T. Hynes, J. Phys. Chem. A **113**, 6657 (2009).
[19] R. Rey and J. T. Hynes, Phys. Chem. Chem. Phys. **14**, 6332 (2012).
[20] S. Imoto, S.S. Xantheas, and S. Saito, J. Chem. Phys. **138**, 54506 (2013).
[21] S. Ashihara, N. Huse, A. Espagne, E.T.J. Nibbering, and T. Elsaesser, Chem. Phys. Lett. **424**, 66 (2006).
[22] J. Lindner, P. Vöhringer, M.S. Pshenichnikov, D. Cringus, D.A. Wiersma, and M. Mostovoy, Chem. Phys. Lett. **421**, 329 (2006).
[23] S. Ashihara, S. Fujioka, and K. Shibuya, Chem. Phys. Lett. **502**, 57 (2011).
[24] L. Chuntonov, R. Kumar, and D.G. Kuroda, Phys. Chem. Chem. Phys. **16**, 13172 (2014).
[25] J. Lindner, D. Cringus, M.S. Pshenichnikov, and P. Vöhringer, Chem. Phys. **341**, 326 (2007).
[26] S. Ashihara, N. Huse, A. Espagne, E.T.J. Nibbering, and T. Elsaesser, J. Phys. Chem. A **111**, 743 (2007).
[27] J. Diels and W. Rudolph, *Ultrashort Laser Pulse Phenomena* (Academic Press, San Diego, 1996).
[28] P.B. Petersen and A. Tokmakoff, Opt. Lett. **35**, 1962 (2010).
[29] J. Helbing and P. Hamm, J. Opt. Soc. Am. B **28**, 171 (2010).
[30] L.P. DeFlores, R.A. Nicodemus, and A. Tokmakoff, Opt. Lett. **32**, 2966 (2007).
[31] L. Mertz, Infrared Phys. **7**, 17 (1967).
[32] C.J. Fecko, J.J. Loparo, S.T. Roberts, and A. Tokmakoff, J. Chem. Phys. **122**, 54506 (2005).
[33] R. Biswas, W. Carpenter, J.A. Fournier, G.A. Voth, and A. Tokmakoff, J. Chem. Phys. **146**, 154507 (2017).
[34] M.J. Frisch, G.W. Trucks, H.B. Schlegel, G.E. Scuseria, M.A. Robb, J.R. Cheeseman, G. Scalmani, V. Barone, B. Mennucci, G.A. Petersson, *et al.* GAUSSIAN 09, Revision D.01,

Gaussian, Inc., Wallingford, CT, USA (2009).
[35] S. Sastry, N. Deo, and S. Franz, Phys. Rev. E. Stat. Nonlin. Soft Matter Phys. **64**, 16305 (2001).
[36] I. Bakó, T. Megyes, and G. Pálinkás, Chem. Phys. **316**, 235 (2005).
[37] D. Cringus, T.L.C. Jansen, M.S. Pshenichnikov, and D.A. Wiersma, J. Chem. Phys. **127**, 84507 (2007).
[38] F. Dahms, R. Costard, E.T.J. Nibbering, and T. Elsaesser, Chem. Phys. Lett. **652**, 50 (2016).
[39] Y. Ni and J.L. Skinner, J. Chem. Phys. **143**, 14502 (2015).
[40] M. Khalil, N. Demirdöven, and A. Tokmakoff, J. Phys. Chem. A **107**, 5258 (2003).
[41] O.F.A. Larsen and S. Woutersen, J. Chem. Phys. **121**, 12143 (2004).
[42] N. Huse, S. Ashihara, E.T.J. Nibbering, and T. Elsaesser, Chem. Phys. Lett. **404**, 389 (2005).
[43] G.E. Walrafen and L.A. Blatz, J. Chem. Phys. **59**, 2646 (1973).
[44] M. Moskovits and K.H. Michaelian, J. Chem. Phys. **69**, 2306 (1978).
[45] B. Zelent, N. V. Nucci, and J.M. Vanderkooi, J. Phys. Chem. A **108**, 11141 (2004).
[46] V. Kemlin, A. Bonvalet, L. Daniault, and M. Joffre, J. Phys. Chem. Lett. **7**, 3377 (2016).
[47] M.C. Thielges and M.D. Fayer, J. Phys. Chem. A **115**, 9714 (2011).
[48] A.J. Lock, S. Woutersen, and H.J. Bakker, J. Phys. Chem. A **105**, 1238 (2001).
[49] T. Steinel, J.B. Asbury, J. Zheng, and M.D. Fayer, J. Phys. Chem. A **108**, 10957 (2004).
[50] Z. Wang, Y. Pang, and D.D. Dlott, J. Phys. Chem. A **111**, 3196 (2007).
[51] H.J. Bakker, Y.L.A. Rezus, and R.L.A. Timmer, J. Phys. Chem. A **112**, 11523 (2008).
[52] Y.L.A. Rezus and H.J. Bakker, J. Chem. Phys. **125**, 144512 (2006).
[53] P. Foggi, P. Bartolini, M. Bellini, M.G. Giorgini, A. Morresi, P. Sassi, and R.S. Cataliotti, Eur. Phys. J. D **21**, 143 (2002).
[54] M.G. Sceats, M. Stavola, and S.A. Rice, J. Chem. Phys. **71**, 983 (1979).
[55] Z. Wang, A. Pakoulev, Y. Pang, and D.D. Dlott, J. Phys. Chem. A **108**, 9054 (2004).
[56] G. Seifert, T. Patzlaff, and H. Graener, J. Chem. Phys. **120**, 8866 (2004).
[57] Y.S. Lin, S.G. Ramesh, J.M. Shorb, E.L. Sibert, and J.L. Skinner, J. Phys. Chem. B **112**, 390 (2008).
[58] J.A. Fournier, W. Carpenter, L. De Marco, and A. Tokmakoff, J. Am. Chem. Soc. **138**, 9634 (2016).
[59] S. Woutersen and H.J. Bakker, Nature **402**, 507 (1999).
[60] H. Torii, J. Phys. Chem. A **110**, 9469 (2006).
[61] T. Yagasaki, J. Ono, and S. Saito, J. Chem. Phys. **131**, 164511 (2009).
[62] M.J. Gillan, D. Alfe, and A. Michaelides, J. Chem. Phys. **144**, 130901 (2016).
[63] M. Heyden, J. Sun, S. Funkner, G. Mathias, H. Forbert, M. Havenith, and D. Marx, Proc. Natl. Acad. Sci. U. S. A. **107**, 12068 (2010).
[64] T. Yagasaki and S. Saito, J. Chem. Phys. **134**, 184503 (2011).
[65] T. Yagasaki and S. Saito, J. Chem. Phys. **128**, 154521 (2008).
[66] K. Ramasesha, S.T. Roberts, R.A. Nicodemus, A. Mandal, and A. Tokmakoff, J. Chem. Phys. **135**, 54509 (2011).
[67] T. Yagasaki and S. Saito, Annu. Rev. Phys. Chem. **64**, 55 (2013).
[68] T. Yagasaki and S. Saito, Acc. Chem. Res. **42**, 1250 (2009).
[69] T.I.C. Jansen, J.G. Snijders, and K. Duppen, J. Chem. Phys. **113**, 307 (2000).
[70] T. Hasegawa and Y. Tanimura, J. Chem. Phys. **125**, 74512 (2006).
[71] B. Miguel, J. Zúñiga, A. Requena, and A. Bastida, J. Phys. Chem. B **118**, 9427 (2014).
[72] P. Hamm and G. Stock, Phys. Rev. Lett. **109**, 173201 (2012).